Microstructural Variations in a High-Strength Structural Steel Weld under Isoheat Input Conditions

Weld bead morphologies influence weld cooling rate and hence the acicular ferrite content in steel

BY B. BASU AND R. RAMAN

ABSTRACT. Bead-in-groove submerged arc welding of quenched and tempered (Q & T) HSLA steel using a suitable welding wire and an agglomerated basic flux (basicity index = 3.1) was carried out under heat input conditions varying from 1.9 to 3.7 kJ/mm. The heat input was adjusted by varying the welding current and welding speed with the machine operated in the constant voltage mode (32–33 VDC). From several welds prepared using a range of currents (400–800 A) and speeds (3–13 mm/s), nine welds were selected. These welds represented those prepared under isoheat input conditions with different current and speed combinations. It was found all the parameters (namely, prior austenitic grain size, inclusion characteristics, cooling rate) influencing the volume fraction of intragranularly precipitated acicular ferrite in the weld showed significantly different dependence at a particular heat input depending upon the welding current and speed combination used. A new cooling rate parameter (NA/C1) based on the weld nugget cross-sectional area (NA) and the fusion zone/heat-affected zone interface length (C1) were defined. Using multiple regression analysis, a correlation between acicular ferrite content and the different influencing parameters as mentioned above was defined having ~90% correlation coefficient. This correlation can be utilized in setting up the trial welding parameters for similar grades of steel substrates and consumables with an aim to maximizing the acicular ferrite content.

Introduction

In the use of high-strength steels for structural applications, the greatest concern is achievement of the desired mechanical properties in the weld, particularly low-temperature toughness. To economically achieve the required combination of high strength and excellent low temperature toughness in welds for constructional applications, appropriate selection of welding parameters must be addressed. It is a common practice to correlate the various weld metal properties with heat input. Thus, the effects of individual welding parameters such as current and speed are not properly assessed when combined in the form of heat input. The effects of variation of welding current and speed are expected to result in subtle variations in microstructure leading to mechanical properties anywhere between highly desirable to highly deleterious, even though welding might have been carried out using the same heat input. Published information (Refs. 1–4) is available in a very general manner on the effect of welding parameters, particularly heat input, on the structure and properties of high-strength steel welds. However, the effects of individual welding parameters, like current and speed, on the various microstructural and mechanical properties have hardly been systematically addressed, particularly under isoheat input conditions.

It is well established that weld microstructure containing intragranularly formed acicular ferrite, due to its fine basket-weave-like structure, helps to achieve good low-temperature toughness (Refs. 5–8). Extent of formation of such a structure is a result of competition with undesirable higher temperature ferrite morphologies and involves the complex interaction between welding parameters, plate and welding wire chemistry, flux composition, and, significantly, the actual cooling rate the weld experiences. Using the classical approach (Ref. 9) of heat flow in fusion welding, it is possible to estimate the cooling rate experienced by the weld. However, these estimates are rarely accurate, especially with respect to the fusion zone. This is because these empirical equations do not take into account the weld nugget macromorphology that is expected to play a decisive role in the weld cooling rate. Further, the macromorphologies of the weld nugget are expected to depend on the individual welding parameters and cannot be accurately correlated with heat input. In this work, an attempt has been made to study microstructural variations in a submerged arc weld of a high-strength steel under different isoheat input conditions.

KEY WORDS

Submerged Arc Welding
HSLA Steel
Isoheat Input Conditions
Acicular Ferrite
Grain Boundary Ferrite
Polygonal Ferrite
Ferrite Side Plate
CCT Diagram

B. BASU is Scientist, Naval Materials Research Laboratory, Naval Dockyard, Mumbai, India. R. RAMAN is Professor, Metallurgical Engineering and Materials Science Department, Indian Institute of Technology – Bombay, Mumbai, India.

Experimental

The objective of the present work is to study the effects of heat input, as a whole, and individual welding parameters such as welding current and speed, under isoheat input conditions, on the microstructural variations of as-deposited weld metal obtained by single-pass, bead-in-groove welding. The single-pass, bead-in-groove welds were characterized for chemistry including oxygen, volume fraction of various microstructural phases, sizes of prior austenitic grains, and inclusion characteristics.

Materials

Base plate — A 22-mm-thick HSLA steel was used for the experiment.

Welding Wire — A 3.15-mm-diameter, copper-coated alloyed wire was used as welding wire. Chemical analysis of the base plate and the welding wire used in the experiments is shown in Table 1.

Flux — A highly basic, commercially available agglomerated flux with basicity 3.1 was used to carry out the welding. To drive away the moisture absorbed during stor-

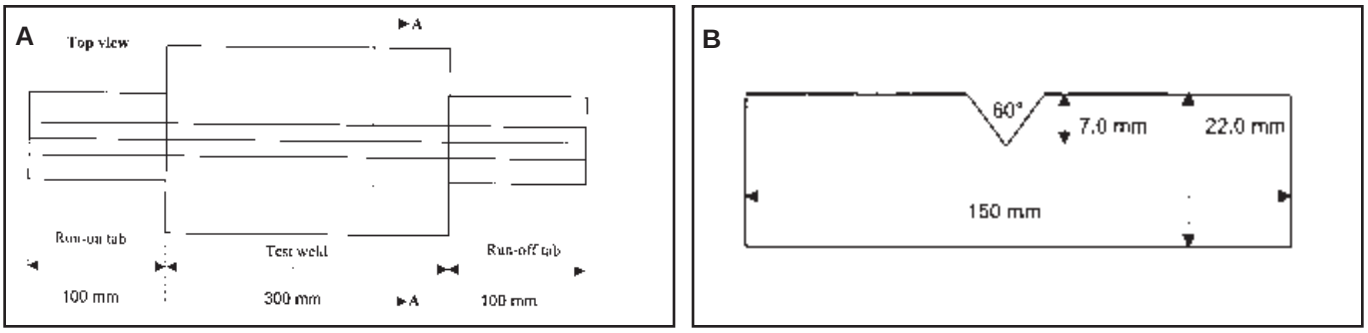

Fig. 1 — Schematic of the joint geometry. A — Top view; B — side view (section AA).

Table 1 — Chemical Composition (wt-%) of Base Metal and Welding Wire

Elements	C	Si	Mn	Ni	Cr	Mo	S	P	Cu
Base Metal	0.08	0.23	0.4	1.8	0.44	0.29	<0.01	<0.01	0.38
Welding Wire	0.04	0.1	0.81	2.6	0.07	0.24	<0.01	<0.01	0.11

Table 2 — Chemical Composition of Flux

Constituents	MgO	CaF_2	SiO_2	Al_2O_3	TiO_2	MnO	CaO
Wt-%	36	26	13	12	0.5	0.5	12

Table 3 — Welding Parameters

Code	Current (Amp)	Speed (mm/s)	Heat Input (kJ/mm)
E	425	7.00	1.97
F	425	4.75	2.91
G	425	3.70	3.73
I	625	10.83	1.87
D	625	7.00	2.90
C	625	5.45	3.72
H	800	13.90	1.87
J	800	8.90	2.92
K	800	7.00	3.71

age, the flux was heated in a drying oven at 350°C for 2 h just before use. The approximate composition of the flux constituents is shown in Table 2.

Weld Preparation

Joint Geometry — The plates were ground to a bright metal finish before depositing the beads. Single-pass, bead-in-groove welds were made on 22-mm-thick, 360- x 150-mm steel plates using submerged arc welding (SAW). A SAW machine in constant voltage mode carried out the welding. The joint geometry used for carrying out the test welds is shown in Fig. 1. The run-on tabs allowed enough time to adjust welding current and voltage, while the run-off tabs prevented crater formation within the actual weld of interest. Thus, for each deposit, 300-mm-long deposits of acceptable quality could be achieved.

Welding Parameters — A series of submerged arc welds was produced using a range of heat inputs from 2 to 4 kJ/mm at varying current levels from 425 to 800 A. Since a large amount of mechanical, metallurgical, and chemical characterization work was to be done, nine welds were selected from a number of experimental welds. The basis for selection was to include as wide a range of welding speeds as possible. The nine welds selected for analysis represented three heat input levels at three current levels, as illustrated in Table 3. This selection made it possible to study the properties of various welds under isoheat input conditions but with different combinations of individual welding parameters, specifically current and speed. Submerged arc welding was performed using direct current, electrode positive with an initial electrode extension of 22 mm, under constant voltage. Welding voltage was kept constant at 32–33 V for all welding trials.

Characterization of the Welds

The prepared welds were separated from the run-on and run-off tabs. The separated welds were used for chemical elemental analysis including oxygen content, quantitative metallography, inclusion characteristics, and weld bead morphology.

Chemical Analysis — Chemical composition of the as-received base plate and core wire were obtained using an emission spectrometer for the elements manganese, silicon, nickel, chromium, copper, vanadium, and phosphorus and using an interstitial combustion analyzer for carbon and sulfur. Oxygen and nitrogen analysis of the samples was carried out using an infrared oxygen analyzer. The samples for oxygen and nitrogen analysis were taken from the center of the welds and carefully machined using a cooling solution into small cylindrical specimens 2 mm in diameter and 5 mm in length. The chemical analysis, including oxygen, was the average of three results.

Quantitative Metallography — Quantitative metallography was carried out using an inverted microscope attached with an image analyzer. The experimental welds were sectioned transverse as well as inclined to the welding direction for metallographic examination, as shown in Fig. 2. Sectioning of the samples for quantitative metallography was done near the middle of the length of the weldment, at two different locations. Due to distortion during sectioning, the measurement on a transverse section may not give the true prior austenitic grain size. Therefore, inclined sections, perpendicular to the columnar grains, were prepared and approximately equiaxed austenite grains were observed and measured. The size of the prior austenite grains was measured by tracing along individual grains and measuring the enclosed area using a computerized image analyzer. More than 100 prior austenite grains were measured from 5 to 10 different fields for all the individual welds. The specimens were mechanically polished to a 0.25-μ diamond finish in an

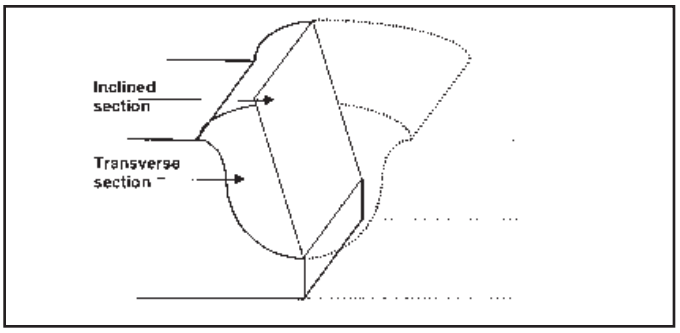

Fig. 2 — Schematic showing the sample preparation for microstructural characterization. (Inclined section — prior austenitic grain size determination; transverse section — microstructural observation.

Fig. 3 — Schematic of weld bead showing different bead morphologies.

Table 4 — Chemical Composition of Experimental Welds

Code	C	Mn	Si	S	P	Ni	Cr	Mo	Cu	O (ppm)	N (ppm)	P_{cm}
E	0.077	0.77	0.22	0.009	0.020	2.47	0.24	0.25	0.47	394	146	0.216
F	0.055	0.77	0.21	0.006	0.020	2.60	0.23	0.25	0.47	335	117	0.195
G	0.054	0.78	0.19	0.007	0.023	2.41	0.22	0.25	0.45	378	130	0.189
I	0.070	0.76	0.22	0.005	0.021	2.50	0.25	0.26	0.51	454	127	0.212
D	0.064	0.73	0.23	0.006	0.019	2.47	0.26	0.25	0.49	404	124	0.203
C	0.063	0.75	0.24	0.006	0.020	2.46	0.24	0.25	0.49	340	136	0.203
H	0.075	0.77	0.25	0.005	0.016	2.31	0.24	0.25	0.50	457	161	0.214
J	0.065	0.77	0.23	0.005	0.018	2.61	0.27	0.26	0.45	403	126	0.208
K	0.064	0.77	0.22	0.005	0.018	2.63	0.24	0.25	0.47	383	140	0.206

automatic polisher. The weld metal microstructure was revealed by etching with a freshly prepared 2% nital solution. The volume fraction of different microstructural constituents, namely, grain boundary ferrite (GBF), polygonal ferrite (PF), ferrite side plate (FSP), and acicular ferrite (AF), were obtained from more than 500 point counts carried out at a magnification of 500X on a transverse section.

Inclusion Analysis — Measurement of volume fraction of nonmetallic weld metal inclusions was carried out on transverse sections of the welds. The polished samples were observed without etching at 1500X magnification under an optical microscope attached with an image analyzer. More than 500 inclusions from various fields were taken for quantitative analysis. Due to limitations in the accuracy of detection levels of the optical microscope, inclusions having a diameter of less than 0.20 μ were not considered for analysis.

Weld Nugget Morphology — The morphology of the weld nuggets was measured from samples in the direction transverse to the welding direction. Sectioning of the samples was done at the center of the length of the weld nuggets. Nugget morphologies were measured by tracing an enlarged (10X) image of the polished and macroetched section of the weld profile using a profile projector. The various nugget morphologies measured, as per the schematic of weld bead dimensions shown in Fig. 3, were nugget area (NA) mm^2 and fusion zone boundary length (C1) mm.

Results

Weld Chemical Analysis

The chemical compositions of the experimental welds are given in Table 4.

Weld Bead Morphology

The weld nugget morphologies have been tabulated in Table 5. It is assumed the weld nugget cross section is the same throughout the weld length. Hence, the nugget area (NA) (considering unit length of weld) can be assumed to represent the amount of metal fused and the amount of heat to be extracted by the surrounding base metal. In SAW, the cooling of the weld essentially takes place due to the surrounding base metal and, therefore, the fusion zone/HAZ boundary length (C1) (again considering unit length of weld) can be assumed to represent the area through which the heat is transferred. It has been observed that with an increase in current, at each of the three heat input levels, the nugget area increases — Fig. 4. The fusion zone boundary length (C1) was observed to increase with current at all heat input levels (Fig. 5) except at the highest current and highest heat input combination.

Prior Austenite Grain Size (g)

The variations in austenitic grain sizes (g) with current under isoheat input conditions are listed in Table 5 and shown in Fig. 6. It should be noted the values given are the average of about 100 measurements from different fields done on each weld. Typical micrographs with clearly delineated prior austenite grains are shown in Fig. 7A–C.

Volume Fraction of Various Phases

Classification of various phases present in the weld was done by IIW method, based on the recommendations of Abson and Pargeter (Ref. 10). The different phases identified and quantified were acicular ferrite, grain boundary ferrite, polygonal ferrite, and ferrite side plates. From the results (Table 6), it can be seen the volume fraction of AF, in general, is quite high and varied between 67 and 84%. It is interesting to note (Fig. 8) that acicular ferrite content shows significant differences in dependence on the welding current although heat input remains the same. This is particularly so at higher levels of welding current at which the weld bead morphology is likely to change significantly due to increased penetration. This is likely to affect cooling rate significantly, as will be explained later, and, hence, AF content. The microstructures showing various phases of the welds are shown in Fig. 9A–C.

Inclusion Analysis

Inclusion analysis was done using an optical microscope coupled to an image

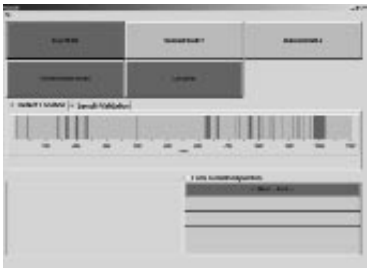

Fig. 4 — Variation of nugget area with current under isoheat input conditions.

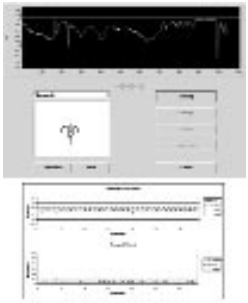

Fig. 5 — Variation of fusion zone boundary length (C1) with current under isoheat input conditions.

Table 5 — Bead Morphology and Prior Austenite Grain Size of Experimental Welds

Code	Nugget Area NA (mm^2)	Fusion Zone Boundary Length C1 (mm)	Grain Size (μ)
E	72.4	22.1	99.3
F	102.0	26.7	130.0
G	120.2	28.2	155.5
I	80.6	25.2	95.0
D	124.0	27.6	135.7
C	177.5	34.8	146.9
H	100.8	26.5	89.0
J	127.0	30.5	110.0
K	181.4	32.3	132.0

Table 6 — Volume Fraction of Various Microstructural Phases and Inclusion Analysis in Experimental welds

	Volume fraction of various phases (%)					
Code	AF	GBF	PF	FSP	Inclusion Size (3-D), dv(μ)	Volume Percent (3-D), f(%)
E	77.6	17.2	1.6	3.6	0.495	0.00146
F	70.6	22.6	2.0	4.8	0.504	0.00148
G	67.0	27.2	1.0	4.8	0.547	0.00229
I	73.8	19.1	3.1	4.0	0.439	0.00264
D	71.6	21.2	2.4	4.8	0.485	0.00171
C	68.0	25.1	2.6	4.3	0.495	0.00158
H	79.7	16.4	2.1	2.8	0.458	0.00235
J	84.0	14.0	1.0	1.0	0.476	0.00137
K	76.7	18.0	3.1	2.2	0.505	0.00124

analyzer. However, the photographs shown in Fig. 10A–C are SEM images of the polished and unetched surface of the weld cross section showing the presence of inclusions. The measured size (average diameter) and volume fraction of inclusions are as listed in Table 6 and graphically shown in Fig. 11A–C. There is a distribution of inclusion sizes. Further details on inclusion distribution will be discussed in a subsequent paper primarily focusing on the aspects of weld metal inclusions. The term 3-D means inclusion analysis done in three dimensions, i.e., volumetric. It is well known formation of intragranular acicular ferrite crucially depends on the presence of an optimum amount of inclusions. It is seen from the figures the inclusion content significantly differs in welds made under isoheat input conditions but with different combinations of current and speed.

Discussion

It is well established (Refs. 5–8) that the toughness of ferrous welds is dependent on the presence of a microstructure predominantly consisting of intragranularly formed acicular ferrite (AF). This is because of a basket-weave-type morphology, 1–3 μ in size, with high angle boundaries and random orientation. This morphology makes the AF inherently resistant to crack propagation (Ref. 8) and to have low transition temperature values. On the other hand, presence of large proportions of upper bainite, ferrite side plates, or grain boundary ferrite are considered to be detrimental to toughness. These structures provide easy crack propagation paths, especially when continuous films of carbides are present between ferrite laths or plates.

The final microstructure developed as a result of welding is principally governed by the relative position of the continuous cooling transformation (CCT) diagram for the particular weld metal and the actual weld cooling curve. The position of the CCT curve will depend on the carbon content, percentage of hardenability elements, prior γ grain size, and the presence of inclusions. It should be noted, in general, the role of hardenability elements is to delay the transformation (shift the CCT curve to the right). On the other hand, an increase in inclusions favors the transformation (shift the CCT curve to the left). The higher the prior austenite grain size, the more the CCT curve will be shifted toward the right and vice versa. For a given weld composition and cooling rate, the type of microstructure will essentially depend on the level of inclusions and prior γ grain size. Thus, development of a weld microstructure is a result of complex interaction between the material being welded, its thickness, and different welding parameters, as schematically depicted in Fig. 12. It should be stressed the overall conditions required to obtain predominantly AF structure lie in between those that promote martensite and bainite type of transformation (faster rate of cooling and shifting of cooling CCT curve to longer periods) and those that promote formation of α (slower cooling rate and shorter periods). It is apparent conditions

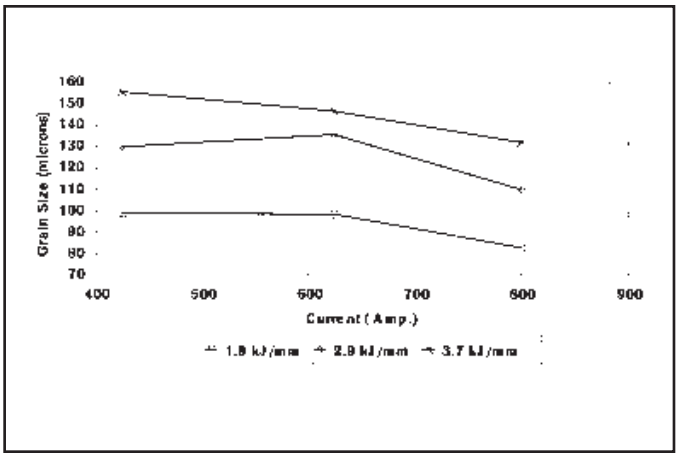

Fig. 6 — Variation of prior austenitic grain size with current under isoheat input conditions.

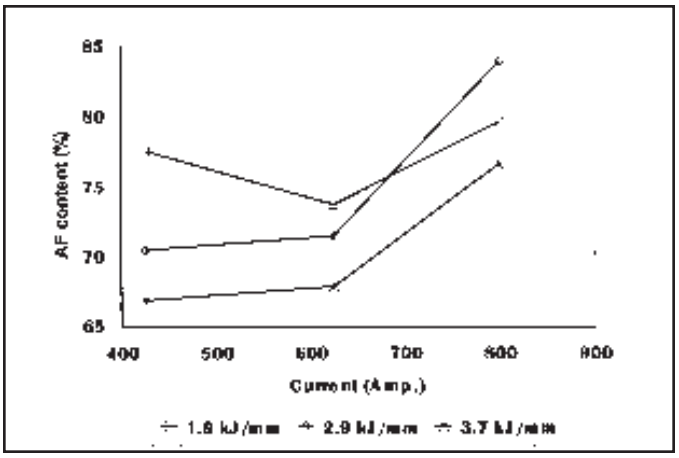

Fig. 8 — Variation of acicular ferrite content with current under isoheat input conditions.

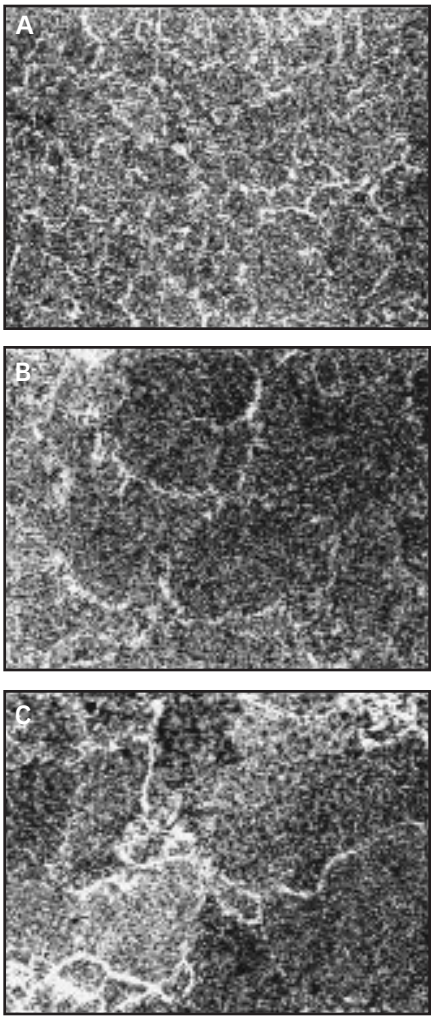

Fig. 7 — Micrographs showing prior austenite grains. A — Weld H (100X); B — Weld C (100X); C — Weld G (63X).

Table 7 — Interdependency of Factors

	NA/C1 Ratio	Prior γ Grain Size, g (mm)	Inclusion vol. fr., f (%)	Inclusion Size, dv (μ)
NA/C1 ratio ↑	—	↑	↓	↑
Prior γ Grain Size ↑ g (mm)	—	—	↓	↑
Inclusion vol. fr., ↑ f (%)	—	↓	—	—
Inclusion Size, ↑ dv (μ)	—	↑	—	—

for maximizing AF require optimization of various interrelated parameters.

In the present case, variation in the weld compositions obtained during various welding trials was not significant (dilution varied between 50 and 60%) except in the case of carbon content. The minimum carbon content was 0.054% (Weld G) and maximum 0.077% (Weld E). However, for most of the welds, carbon content was between 0.063 and 0.075%. An increase in carbon content is known to shift the CCT curve to longer times. However, this effect has not been considered significant as compared to other parameters because the differences in the carbon contents of the welds are not very large, especially in view of the presence of other alloying elements that contribute to hardenability. Thus, the CCT curve, as far as the role of hardenability elements are concerned, can reasonably be assumed to be fixed. Hence, one needs to essentially consider the prior austenite grain size and the volume fraction of inclusions found in different welds, both of which showed substantial variations in different welds (Tables 5, 6).

Last, but not least, the actual cooling rate experienced by the weld should be considered. It is important to know in studying the effect of welding parameters, for convenience' sake, the parameters are usually combined and expressed as heat input. This approach, although practical, may not reflect the individual effects of the various welding parameters, which could be significant and might vary under identical heat input conditions. This important aspect is clearly seen in Figs. 4–6, 8, and 11, wherein there is significant difference in the results (nugget parameters, γ grain size, etc.) obtained under identical heat inputs but with different welding current and speed combinations. This implies the cooling rate the weld experiences may not have a monotonic dependence on heat input, especially when the welding current is high.

From Fig. 4 and Table 5, it is clear with an increase in current there is an increase in NA. The NA will depend on penetration and the factors that tend to increase width and reinforcement. At the highest heat input, a sharp increase is also noted in NA when going from 425 to 625 A. However, from 625 to 800 A, the change is not significant. Thus, it is seen under constant heat input conditions a wide variation in nugget area is obtained and the variation increases as heat input is increased. Under these conditions, it is unrealistic to expect similar weld metal properties when the same heat input but different welding current and speed combinations are used.

Dependence of Heat Extraction from FZ on the Weld Nugget Morphology

Empirical expressions for weld cooling

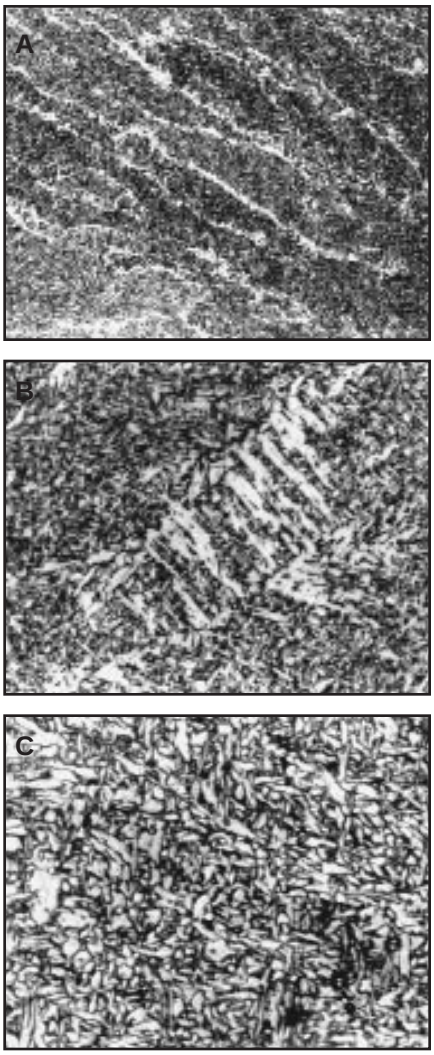

Fig. 9 — A — Micrograph showing GBF in Weld E (250X); B — micrograph showing FSP in Weld G (500X); C — micrograph showing AF in Weld J (1000X).

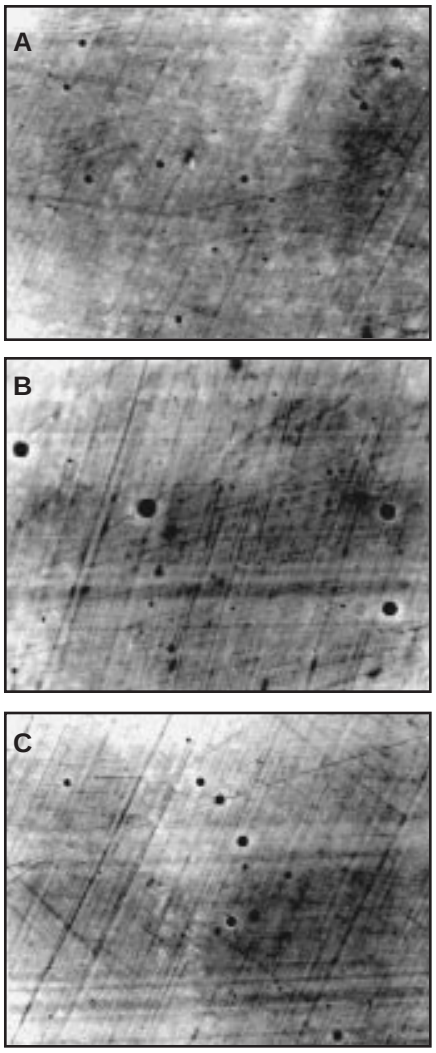

Fig. 10 — Micrographs showing weld metal inclusions. A — Weld I (3000X); B — Weld G (3000X); C — Weld K (3000X).

rate available as thick and thin plate solutions (Refs. 9, 11) do not take into account the effect of the wide variety of nugget morphologies obtainable under the same heat input but with different welding speed and current combinations. These solutions do not agree with the actual weld cooling rates measured (Ref. 12). A simple approach is presented here introducing the concept of NA/C1 ratio (Ref. 13). In the conventional approach, the cooling rate is qualitatively thought to be directly proportional to the effective plate thickness and inversely proportional to the heat input. In the present approach, the cooling rate the weld actually experiences is thought to be related to NA/C1. With increasing current at constant heat input, welding speed is required to be increased proportionately. This leads to an increase in the dimensionless operating parameter, n, given by $n = HI \times v^2/k$; where k is a material-related constant involving thermophysical constant properties (Ref. 14). It is established that, with increasing n, weld NA increases. Obviously, melting efficiency will increase for the same heat input. Note the operating parameter is proportional to the square of the welding speed at any given heat input.

As defined earlier, nugget area (NA) quantitatively represents the amount of heat required to be dissipated by the surrounding substrate metal and will depend on heat input in the conventional sense. C1, on the other hand, represents the FZ/HAZ interface available for conducting away the heat that accumulates in the fusion zone. For cooling rate estimation, it is common practice to evaluate effective plate thickness, heat input, thermal diffusivity of the material, and joint geometry. Based on the value of this effective plate thickness, it is assumed the heat transfer in 2-D or 3-D and approximate solutions are used to estimate the cooling rate experienced by the weld. In the present approach, the ratio NA/C1 is proposed to represent the cooling rate. Exclusions of thermophysical properties in this relationship are justified because the same material is being considered in all the welds.

The relationship is not expected to be linear but, with the assumptions made in defining NA and C1, it can be stated the greater the ratio, the lesser the cooling rate and vice versa. The positive feature of this approach is inclusion of the morphological feature of the weld nugget resulting from the particular combinations of welding parameters, which is not possible in the conventional approach (Refs. 13, 15). A plot of NA/C1 vs. current at various heat inputs is shown in Fig. 13. It is clearly unreasonable to expect identical cooling rates for welds prepared with the same heat input but different current and speed combinations.

Maximization of Acicular Ferrite in Microstructure

Development of a weld microstructure consisting predominantly of intragranularly formed acicular ferrite (75% or more) (Ref. 16) has always been the aim when welding carbon and low-alloy steels. It is generally accepted (Ref. 17) achievement of the above depends on favorable disposition of interdependent factors such as the following: prior austenite grain size, presence of optimum volume fraction of potent nucleation sites such as inclusions 0.2–0.5 μ in size, fusion zone chemistry with respect to hardenability elements, and cooling rate actually experienced by the weld. On cooling, the austenite transforms to a variety of micromorphologies as follows (approximate transformation starting temperatures are in parentheses): grain boundary ferrite (~800°C), ferrite side plates (~750°C), polygonal ferrite (~750–650°C), and acicular ferrite (~650°C) (Ref. 7). In addition, a variety of residual phases (Ref. 18), referred to as microphases, consisting of small amounts of martensite, retained austenite, and degenerate pearlite, also form. Usually the transformation to ferrite morphologies is quite efficient and the total amount of residual phases not significant. Since cooling is continuous, the final microstructure will contain many of the previously mentioned phases with the volume percent distribution of each phase decided by the particular combination of interrelated factors mentioned earlier that exist during welding. As suggested in a recent work (Ref. 19), it is useful to visualize a small region in the weld CCT diagram called the acicular ferrite window. If the actual weld cooling curve passes through the fair portion of this window, then acicular ferrite will be maximized. The position of this window will be decided by the first three factors mentioned earlier — Fig. 14. It should be remembered Fig. 14 is just a schematic

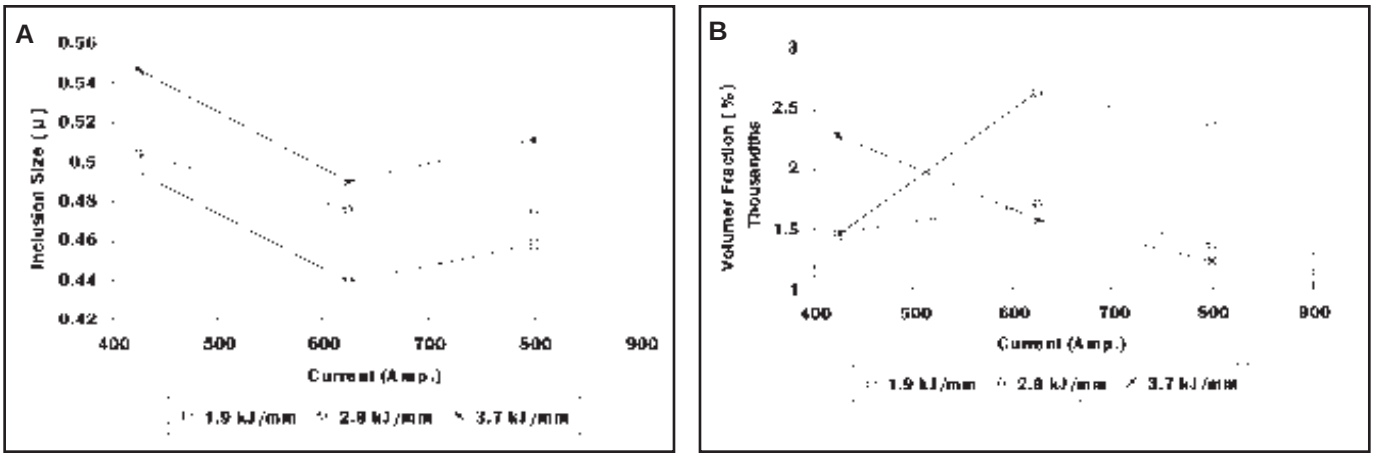

Fig. 11 — A —Variation of inclusion size with current under isoheat input conditions; B — variation of inclusion volume fraction with current under isoheat input conditions.

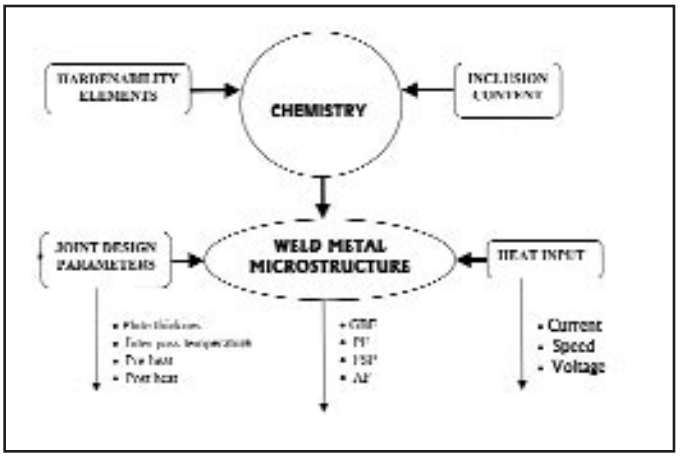

Fig. 12 — The various factors that play a role in deciding weld microstructure.

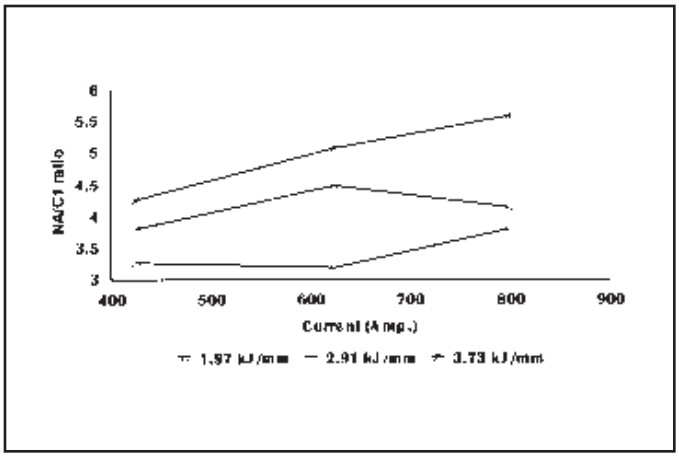

Fig. 13 — Plot of NA/C1 ratio with current under isoheat input conditions.

representation of an ideal situation. The key to maximizing acicular ferrite is for the actual weld cooling rate to avoid the FSP formation zone as far as possible. This is because once FSP is nucleated, it grows at a rapid rate with the growth terminating on soft impingement with other FSP by acicular ferrite. Since all these factors are related to the welding parameters, in principle it should be possible to determine, for a given set of conditions, optimum parameter settings for maximizing acicular ferrite. However, it is essential to first obtain correlation between factors that are responsible for the metallurgical phenomena leading to acicular ferrite formation.

Prior Austenite Grain Size (g)

It is well established (Refs. 20–22) that a minimum prior austenite grain size is required below which formation of acicular ferrite is not favored. The primary reason is the greater availability of grain boundary nucleation and growth sites for the high-temperature diffusional transformation products, i.e., GBF. By the time the kinetics of these reactions slow down parabolically, limited nontransformed austenite is available for the low-temperature displacive process of forming acicular ferrite leading to an inadequate volume fraction of the desirable phase (Ref. 6). As the grain size increases, formation of acicular ferrite is encouraged, provided other factors are favorable. However, above a particular grain size, formation of AF is discouraged due to shifting of the CCT curve to longer times leading to lower temperature transformation products such as bainite and martensite (Ref. 16). The available information suggests an optimum size; however, that would depend on other factors. It has been reported for a certain weld chemistry (low Ti-B welds of low C steels), optimum values lie in the range of 20–60 μ (Ref. 17). From Fig. 6, it is clear prior austenite grain sizes can be significantly different under the same heat input but with different current and speed combinations. This is more pronounced at higher heat inputs. It should also be remembered the size would also depend on the cooling rate represented by NA/C1 and inclusion volume fraction. Lower values of the former and higher values of the latter should lead to smaller grain size. Under isoheat input conditions (Fig. 6), the prior γ grain size decreased with an increase in current level. This indicated for welds made with identical heat inputs but different combinations of welding current and speed, the resultant microstructures may not be the same because the prior γ grain size influences the microstructural transformation to a great extent. This will definitely have its effect, in turn, on the final mechanical properties of the weld metal.

Volume Fraction of Inclusions

It is well established (Ref. 17) that presence of an adequate amount of inclusions of sizes greater than 0.25 μ is necessary to allow the intragranular formation of acicular ferrite. Controversy exists (Refs. 22, 23) as to whether the potency of these inclusions depends on their chemical nature or whether they merely provide inert surfaces to enable the nucleation of the acicular ferrite. However, the following are clear as far as the role of these inclusions:

a) There is no possibility of obtaining any acicular ferrite in the absence of inclusions.

b) The inclusion size should be in the range of 0.25 to 0.50 microns.

c) Inclusions at the grain boundaries have a dual role to play, i.e., smaller ones

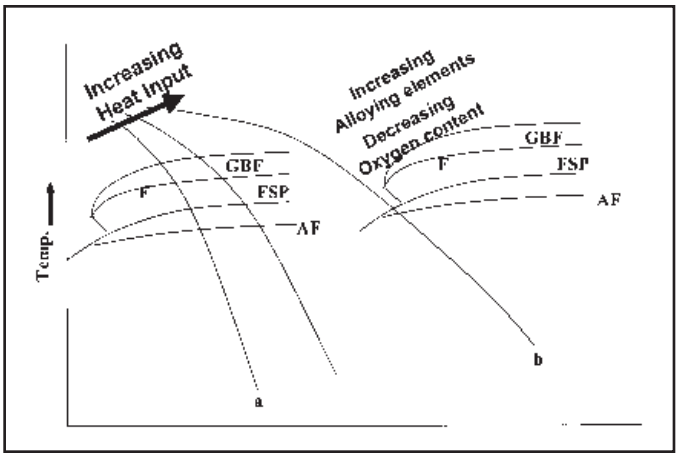

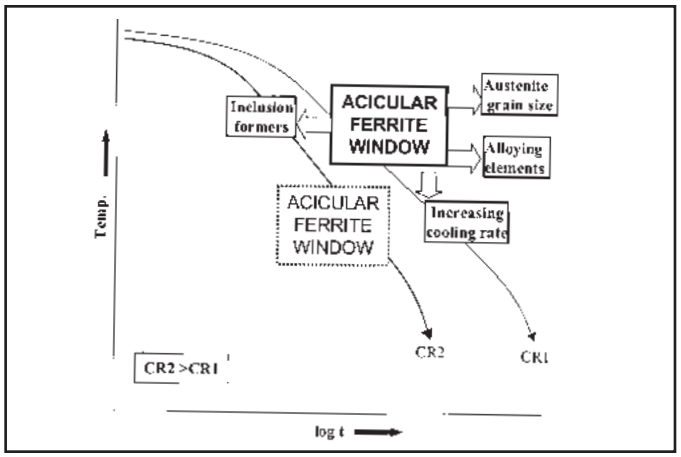

Fig. 14 — Schematic showing the position of the acicular ferrite window and CCT diagram with respect to alloying elements, austenite grain size, and cooling rate.

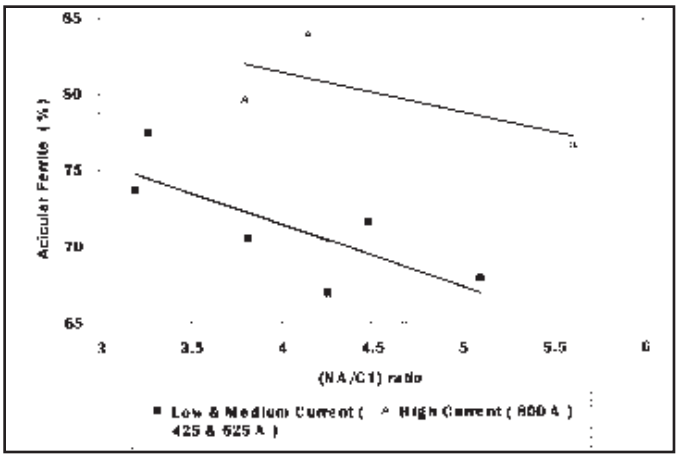

Fig. 15 — Variation of acicular ferrite content with NA/C1 ratio.

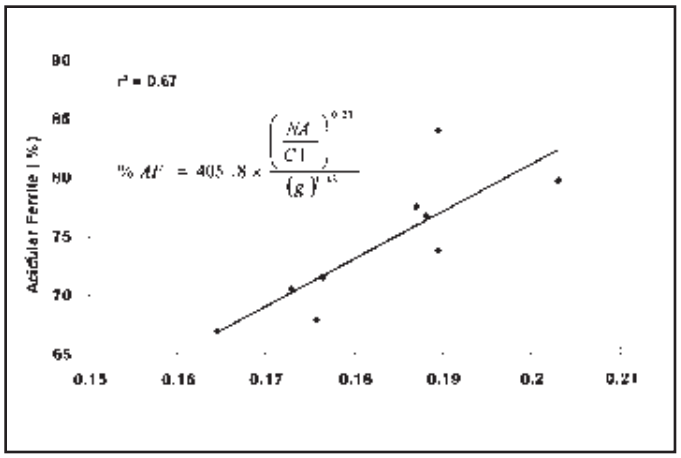

Fig. 16 — Correlation of acicular ferrite content with NA/C1 ratio and prior austenitic grain size.

restrict grain growth and larger ones encourage nonacicular ferrite transformations (both these events are detrimental to the final microstructure formed).

d) The above leads to an upper limit to the desired volume fraction of inclusions.

e) The greater the volume fraction (less than the upper limit), the smaller the interinclusion distances will be and the finer the acicular ferrite plates.

f) Several plates of acicular ferrite can form per inclusion.

As in the case of other metallurgical factors, inclusion characteristics, namely, inclusion size and volume fraction, significantly depend on the welding current and speed combinations used even though carried out at same heat input (see, respectively, Figs. 11A, B). It is seen from these figures and Table 4 there exists some correlation between oxygen content in the weld and inclusion volume fraction, especially at medium and higher heat inputs.

Cooling Rate

Weld cooling rate plays the decisive role in determining weld microstructure. The general effect of increasing the cooling rate is to lower transformation temperatures. When cooled at sufficiently low rates, the microstructure predominantly tends to become polygonal ferrite-pearlite. As the cooling rate is progressively increased, there is a tendency for the polygonal ferrite to be refined and become limited to the prior austenite grain boundaries (Ref. 24). This morphology is often referred to as grain boundary allotriomorphs. Increased cooling rates also reduce, and eventually eliminate, the pearlite phase. The weld microstructure can also show Widmanstatten side plate morphologies that grow out of the large polygonal ferrite grains at low cooling rates or out of the grain boundary allotriomorphs at higher cooling rates. An increased cooling rate tends to increase the ratio of side plates to polygonal ferrite in the final microstructure. It is useful to remember kinetics of side plate growth, which is a displacive phenomena and relies on the instability of the austenite/ferrite interface, is extremely fast as compared to the diffusion-limited parabolic growth rate of grain boundary ferrites. At intermediate cooling rates, provided inclusions are present, intragranular formation of acicular ferrite is encouraged. At still higher cooling rates, the lath ferrite structure, consisting of colonies of parallel laths of ferrite separated by retained austenite or carbides, dominates. Finally, at the highest cooling rates, depending upon the hardenability elements, lath martensite is formed.

Recall, in the present work, cooling rate is represented by NA/C1 and, from Fig. 15, it is clear, at the same heat input, obtaining significantly different microstructure is possible depending upon the welding current and speed combination.

Interdependency of the Factors

It is useful to discuss the interdependency between the three factors discussed previously. It should be noted fusion zone chemistry has not been discussed because it is assumed, since there has not been sig-

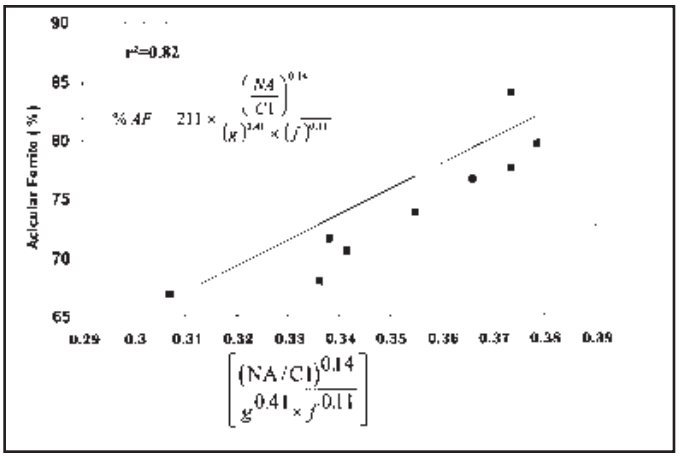

Fig. 17 — Correlation of acicular ferrite content as a function of NA/C1 ratio, prior austenitic grain size, and inclusion volume fraction.

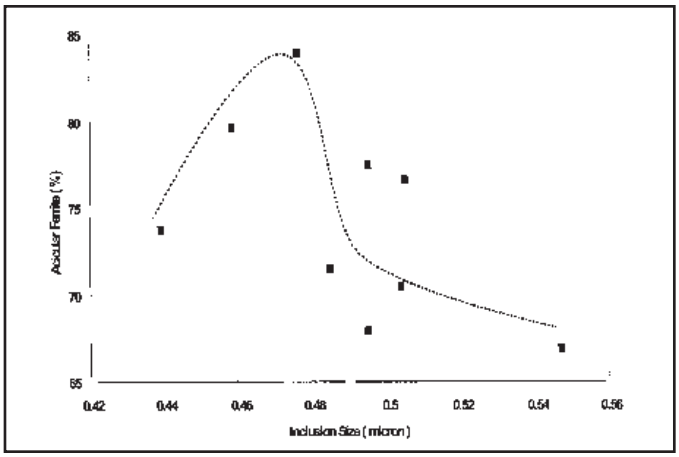

Fig. 18 — Variation of acicular ferrite content with mean inclusion size.

nificant variation in them, with the limited experimental data generated, the discussion will be of a qualitative nature based on basic principles of the welding process. Table 7 shows the matrix of the factors discussed and indicates how each can influence the other.

For higher NA/C1, cooling is slower so the weld will spend a longer time at higher temperatures, leading to larger austenite grain size. At the same time, there will be greater chance for the inclusions to be absorbed by the slag leading to a drop in the volume fraction of inclusions. Furthermore, the average size of the inclusion is likely to be larger. It is unlikely prior austenite grain size is likely to influence the other factors. With respect to inclusion parameters, greater volume fraction will lead to a greater presence of inclusions at the grain boundaries, some of which can act as grain pinning agents and lead to reduction in grain size. As the inclusion size increases, prior austenite grain size will tend to increase because of lesser pinning potential. It is clear from the previous qualitative statements, the cooling rate represented by NA/C1 will have a dominant role to play in deciding the nature of weld microstructure as it appears to affect all the other factors affecting the ultimate weld microstructures.

Dependence of Correlation between Different Factors Responsible for the Formation of Acicular Ferrite

Since NA/C1 appears to play a dominant role in deciding the microstructure, the percentage of acicular ferrite as a function of NA/C1 was plotted as in Fig. 15. It was found necessary to fit the data points corresponding to higher current separately from the data points corresponding to low and medium currents. The figure also shows, for similar cooling conditions, a higher volume fraction of AF is obtained at high currents. This could be related to the fact at higher currents the weld pool is subjected to significantly greater convective flow since the contribution by electromagnetic stirring effects is larger. This can have an effect on the inclusion characteristics leading to different microstructures.

To remove the above separation, other factors, namely, prior austenite grain size (g) and volume fraction of inclusions, were incorporated one by one. The first correlation (Fig. 16) was obtained by performing regression analysis between the percentage of acicular ferrite and the combination of NA/C1 and g. The following correlation was then obtained:

$$\%AF = 405.8 \times \frac{\left(\frac{NA}{C1}\right)^{0.23}}{(g)^{0.43}} \qquad (1)$$

The correlation was not a good one since r^2 was only 0.67. An improvement to $r^2 = 0.82$ was observed by including the volume fraction of inclusions (f) — Fig. 17. The improved relationship was

$$\%AF = 211 \times \frac{\left(\frac{NA}{C1}\right)^{0.14}}{(g)^{0.41} \times (f)^{0.11}} \qquad (2)$$

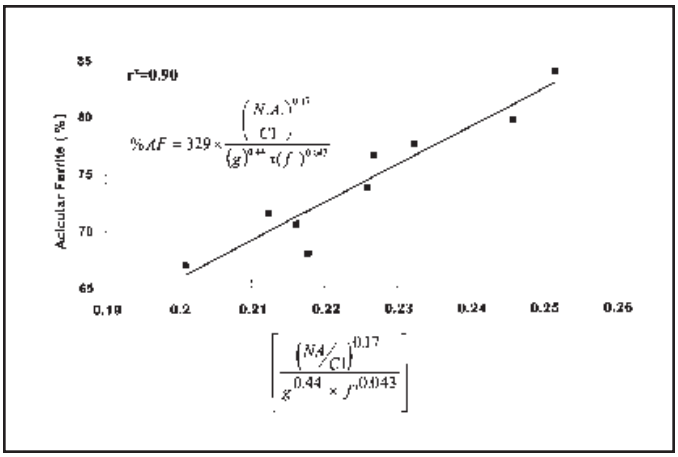

Fig. 19 — Correlation of acicular ferrite content with NA/C1 ratio, austenite grain size (g), and modified volume fraction of inclusions (f').

To further improve the correlation, help was taken from the fact there is a critical range of inclusion size that is likely to be most potent (Ref. 25). From Fig. 18, it can be seen volume fraction of AF is maximized when the sizes of the inclusions are within a range of 0.44 to 0.5 μ. On performing regression analysis between *%AF* and the combination of *NA/C1*, *g,* and f^1 represent the modified volume fraction of inclusions (only inclusions between 0.44 and 0.5 μ were considered), a higher r^2 value of 0.90 was obtained — Fig. 19. The ultimate relationship obtained was

$$\%AF = 329 \times \frac{\left(\frac{NA}{C1}\right)^{0.17}}{(g)^{0.44} \times \left(f^1\right)^{0.043}} \qquad (3)$$

The correlation shown in Equation 3 appears to be reasonably acceptable considering the complexity of the processes involved. The practical utility of the corre-

lation can only be realized when the same can be represented in terms of welding parameters. Each of the terms appearing in Equation 3 has been correlated with welding current and speed (Ref. 13). It was then possible to correlate the AF content with welding parameters. That will form the subject of a subsequent paper. The utility of this correlation for setting up the practical welding parameters appears to be restricted as it involves sectioning of the weld. However, this correlation can serve the purpose of giving starting welding parameters for similar grades of steel substrates and consumables. The magnitude of exponents of the various terms in Equation 3 are possibly indicative of the allowable tolerance of the three main factors responsible for obtaining a given level of AF content in the weld microstructure. Prior austenite grain size appears to be most critical as indicated by a relatively high value of exponent 0.44 as compared to other exponents. A very small value for the exponent on inclusion volume fraction (0.043) does not mean that without the inclusion it is possible to obtain any intragranularly formed AF. All it possibly means is a wide range of inclusion content is acceptable to get the desired AF content in the weld microstructure.

Conclusions

From the present investigation, it is seen significant variations in bead morphology and weld microstructure can occur under identical heat input but with different current and travel speed combinations. From the present investigation, the following major conclusions can be made.

1) Depending upon the welding current and travel speed combinations used, significantly different dependence of all the influencing parameters were observed even though heat input was the same. This can be attributed to differences in the weld bead morphologies. Different weld bead morphologies are likely to lead to different weld cooling rates that will affect the microstructure by itself and also different microstructural features, e.g., austenite grain size, inclusion parameters, that, in turn, will further contribute to the final AF content.

2) A new cooling parameter NA/C1 was found to be a useful representation of the actual weld cooling rate. Rosenthal's work on moving heat source allows expression of the cooling rate based on quantities that can be measured/determined prior to welding (plate thickness, heat input, preheat, etc.). But it need not necessarily represent the true cooling rate because of the empirical nature of defining the heat transfer situation and also in not taking cognizance of the actual bead morphology that forms.

3) Using multiple regression analysis along with other interdependent factors, a correlation between acicular ferrite and the influencing parameters was obtained with a high degree of correlation coefficient. From the magnitude of the exponents of the various terms in the correlation derived, it appears prior austenite grain size is the most critical factor. On the other hand, the low value of the exponent on inclusion volume fraction suggests that, although necessary, some variations in the inclusion volume fraction can be tolerated to obtain a desirable AF content. The magnitude of the exponent on factor NA/C1, which represents the true cooling rate, is intermediate and indicative of greater tolerance than that allowed for prior austenite grain size.

4) The correlation has been derived on the basis of sectioning of the welds. However, the correlation can serve the purpose of obtaining starting welding parameters for similar grades of steel substrates and consumables. For this it is necessary to establish the correlation between various factors and welding parameters (Ref. 13).

5) The full utility of this correlation derived for the present combination of steel substrates and consumables can be realized if realistic mathematical modeling of weld bead morphology, i.e., NA/C1 ratio and microstructural features like prior austenite grain size and inclusion volume fraction can be performed.

References

1. Dixon, B., and Hakansson, K. 1995. Effect of welding parameters on weld zone toughness and hardness in 690 MPa steel. *Welding Journal* 64(4): 122-s.

2. Oldland, P. T., Ramsay, C. W., Matlock, D. K., and Olson, D. L. 1989. Significant features of high-strength steel weld metal microstructures. *Welding Journal* 58(4): 158-s.

3. Smith, N. J., McGrath, J. T., Gianetto, J. A., and Orr, R. F. 1989. Microstructures/mechanical property relationships of submerged arc welds in HSLA 80 steels. *Welding Journal* 58(3): 112-s.

4. Gianetto, J. A., Smith, N. J., McGrath, J. T., and Bowker, J. T. 1992. Effect of composition and energy input on structure and properties of high-strength weld metals. *Welding Journal* 61(11): 407-s.

5. Farrar, R. A., and Zhang, Z. 1995. Aspect ratios and morphology of acicular ferrite in C-Mn-Ni weld metals. *Materials Science Technology* 11: 759.

6. Ricks, R. A., Howell, P. R., and Barritte, G. S. 1982. Nature of acicular ferrite in HSLA steel weld metal. *Journal of Materials Science* 17: 732.

7. Abson, D. J., and Dolby, R. E. 1978. *Weld Inst. Res. Bull.* 19: 202–207,

8. Bhadeshia, H. K. D. H. 1990. *Proc. Conf. on the Metallurgy, Welding and Qualification of Microalloyed (HSLA) Steel Weldments.* Houston, Tex., pp. 34–69.

9. Rosenthal, D. 1941. Mathematical theory of heat distribution during welding and cutting. *Welding Journal* 20(5): 220-s to 234-s.

10. Abson, D. J., and Pargeter, R. J. 1986. Factors influencing as-deposited strength, microstructure and toughness of manual metal arc welds suitable for C-Mn steel fabricators. *International Metals Review* 31(4): 141–194.

11. Easterling, K. 1992. *Introduction to Physical Metallurgy of Welding*. Butterworth-Heineman Ltd., p. 20.

12. Chakraborty, A. P., Thibau, R., and Bala, S. R. 1985. Cooling characteristics of bead-on-plate welds. *Metal Construction* (3): 178 R.

13. Basu, B. 2000. Effect of welding parameters on the structure and properties of a submerged arc weld of a high-strength structural steel. Ph.D. dissertation. IIT – Bombay.

14. Messler, R. W. 1999. *Principles of Welding Processes — Physics, Chemistry and Metallurgy.* John Wiley & Sons Inc., A Wiley Interscience Publication., p. 167.

15. Basu, B., and Raman, R. 2000. Influence of weld bead morphologies on the structure and properties of submerged arc weld metal. Paper No. WM-21, *Symposium on Joining of Materials*, Tiruchirapalli, India.

16. Farrar, R. A., and Harrison, P. L. 1987. Acicular ferrite in carbon-manganese weld metals: An overview. *Journal of Mater. Sci.* 22(11): 3812.

17. Thewlis, G. 1994. Transformation kinetics of ferrous weld metal. *Mater. Science Tech.* 2: 110–125.

18. Honeycombe, Sir. R., and Bhadeshia H. K. D. H. 1995. *Steels — Microstructure and Properties,* p. 280. London, U.K.: Edward Arnold.

19. Yelpale, P. S. 2000. Influence of the presence of active gas in shielding gas mixture on weld quality. M. Tech. dissertation. IIT – Bombay.

20. Grong, O., and Matlock, D. K. 1986. Microstruture development in mild and low-alloy steel weld metals. *Int. Mater. Rev.* 31(1): 27.

21. Ferrante, M., and Farrar, R. A. 1982. The role of oxygen rich inclusions in determining the microstructure of weld metal deposits. *Journal of Mat. Sci.* 17: 3293.

22. Liu, S., and Olson, D. L. 1986. The role of inclusions in controlling HSLA steel weld metal microstructues. *Welding Journal* 55(6): 139-s.

23. Brooksbank, D., and Andrews, K. W. 1972. Stress fields around inclusions and their relation to mechanical properties. *Journal of the Iron and Steel Institute*, pp. 210–246.

24. Harrison, P., and Farrar, R. 1987. Microstructure and toughness of C-Mn and C-Mn-Ni weld metal — Part I. *Metals Construction* 7: 392R–399R.

25. Mills, A. R., Thewlis, G., and Whiteman, J. A. 1987. The nature of inclusions in steel weld metals and their influence on the formation of acicular ferrite. *Mater. Sci. Tech.* 3: 1051–1061.